

Experimental and numerical studies of the pontoon effect on vortex-induced motions of deep-draft semi-submersibles

Mingyue Liu^{a,b}, Longfei Xiao^{a,b,1}, Yibo Liang^c, Longbin Tao^c

^a*State Key Laboratory of Ocean Engineering, Shanghai Jiao Tong University, Shanghai 200240, China*

^b*Collaborative Innovation Center for Advanced Ship and Deep-Sea Exploration, Shanghai 200240, China*

^c*School of Marine Science and Technology, Newcastle University, Newcastle upon Tyne, NE1 7RU, UK*

Abstract

The phenomenon of vortex-induced motion (VIM) is a critical issue for column-type deepwater platforms. As regards to deep-draft semi-submersibles (DDS), even though VIM is mainly excited by vortex shedding around columns, the large-volume pontoons beneath the columns are also responsible for the wake interference, implying a non-negligible influence on VIM behavior. An experimental study and three-dimensional numerical simulations were performed to analyze the pontoon effect on the VIM of two semi-submersibles and a four-column structure. The numerical results acquired using Detached Eddy Simulation (DES) are in good agreement with the experimental measurements obtained from the towing model tests. The present investigations indicate that the resonant phenomenon is observed for all configurations. However, the presence of pontoons delays the onset of VIM to a higher reduced velocity in the cases of the four-pontoon DDS.

¹Corresponding author. Tel.: +86 21 34207050; Fax: +86 21 34207058. E-mail address: xiaolf@sjtu.edu.cn (L. F. Xiao).

1 Additionally, the four-column structure with no pontoons shows the most significant transverse
2 responses and yaw motions at both 0°- and 45°-incidences owing to the largest fluctuating lift forces
3 induced by the well-established wake. The dominant frequency of the drag force for the DDS with
4 two pontoons matches that of the lift force at a 45°-incidence, leading to an increase in the in-line
5 response.

6 **Keywords:** Vortex-induced motion, Deep-draft semi-submersible, Experimental study, Numerical
7 simulation, Pontoon effect

8 **1. Introduction**

9 The semi-submersible platform is one of the most reliable and cost effective structures for
10 offshore oil and gas exploration in deep water. Deep-draft semi-submersible (DDS) concepts are
11 known for their improved vertical motion characteristics compared to conventional semi-
12 submersibles in wave environments owing to the reduced wave exciting forces acting on the
13 pontoon structure and increased heave natural period. However, significant vortex-induced motion
14 (VIM) often occurs in the deep-draft semi-submersible platform as observed on spar platforms,
15 which can cause damaging fatigue stresses on the riser and mooring systems and higher mooring
16 loads for the overall platform as reported by Sagrilo et al. (2009).

17 A number of studies on the VIM behavior of spar and monocolumn platforms have been reported
18 using both model tests and numerical schemes, focusing on the motion characteristics, the excitation
19 current forces, and the influence of various relevant aspects such as the hull geometry and
20 appendages, presence of waves, draft conditions, and motion suppressor. Huang et al. (2003) and
21 Yung et al. (2004) introduced pioneering discussions on the importance of headings in relation to

1 the VIM performance of a spar platform. This influence is directly related to the position of the
2 appendages, fairleads and chains on the hull. van Dijk et al. (2003) and Irani and Finn (2004)
3 reported that waves have also effect on VIM of a spar. In the same sense, Finnigan et al. (2005)
4 presented the first results regarding truss spar VIM in the simultaneous presence of waves and
5 current, which showed that waves in-line with the current direction generally reduce VIM response.
6 Gonçalves et al. (2010b) carried out a battery of VIM tests on a monocolumn platform to evaluate
7 the effect of draft conditions and external damping. The results showed that reducing the immersed
8 portion of the column caused a large mitigation in the VIM response, and the same conclusion can
9 be found in the study on VIV phenomenon of low aspect ratio cylinders described by Gonçalves et
10 al. (2010a). In the attempt to suppress the VIM, serious effort has been made on strake developments
11 fitted to the mono- and multi-column platforms (Finn et al., 2003, Irani and Finn, 2005, and Wang
12 et al., 2010). These experimental works indicated that strakes can be a good solution for minimizing
13 the VIM response of spars, but they need to be carefully designed and tested for each particular
14 platform. On the other hand, Oakley and Constantinides (2007) and Wang et al. (2009) pointed out
15 that the use of Computational Fluid Dynamics (CFD) was a reasonable alternative for selecting the
16 proper configurations of strakes in terms of quantitative analysis.

17 The geometry of semi-submersibles, i.e., multi-column and multi-pontoon, implies a more
18 complex VIM phenomenon than that of single cylindrical structures, such as spar and monocolumn
19 platforms. The confirmed presence of VIM on deep-draft semi-submersibles was found in field
20 measurements by Rijken and Leverette (2009) and Ma et al. (2013). Waals et al. (2007) performed
21 VIM tests on both semi-submersibles and tension-leg platforms (TLPs) to examine the influences
22 of the mass ratio, draft conditions, and pontoons. The TLP model showed a wider range of high

1 amplitude response in the transverse direction owing to a lower mass ratio; furthermore, significant
2 yaw amplitudes, which were not thoroughly discussed in the VIM studies on cylindrical platforms,
3 were observed for multi-column floaters. A seakeeping model test of a DDS was carried out by
4 Hong et al. (2008) to assess its global motion performance in wind, wave, and current environments.
5 Although the test was not specifically for the VIM of the DDS model, it was observed that a DDS
6 with deeper draft experiences more significant VIM with predictable oscillation period and the VIM
7 amplitude in strong current tends to be larger than that for the combination of currents and waves.
8 Rijken and Leverette (2008) experimentally investigated the VIM responses of a DDS in the
9 presence of a fatigue sea state and supported by a system with increased sway damping, which
10 delayed the onset of VIM to a higher reduced velocity. Additionally, Rijken et al. (2011) analyzed
11 the effects of a SCR system and hull appurtenances on the VIM behavior of a DDS with square
12 columns and observed the differences in VIM response between model tests and field observations.
13 Only appurtenances located on the vertical faces of the column and above the pontoon level appears
14 to alter the VIM response. In the same line of research, Goncalves et al. (2012, 2013) performed a
15 series of VIM tests on a semi-submersible to verify the influences of relevant factors such as the
16 current incidence angle, hull appendages, draft condition, external damping, and surface waves.

17 Furthermore, Rijken (2014) examined the influences of mass ratios, scale, and column shapes on
18 the VIM performance of a semi-submersible through CFD analysis and stated that the two-
19 dimensional (2-D) numerical simulation failed to accurately model the VIM response. Tan et al.
20 (2013) discussed in detail the numerical methodology for VIM study of a multi-column floater and
21 proposed some parameters to improve the simulation accuracy. It is revealed that the better
22 agreement between numerical results and corresponding experimental results can be achieved for

1 higher reduced velocities. Kim et al. (2011) and Lee et al. (2014) also employed CFD method to
2 investigate the VIM phenomenon of semi-submersible platforms.

3 VIM of a semi-submersible is induced by the fluctuating hydrodynamic forces stemming from
4 the alternating eddies or vortices shed downstream from one side to the other of each platform
5 column. Thus, the flow interference of multi-cylinder arrays is vital in understanding the VIM
6 behavior of semi-submersibles subject to currents. Zdravkovich (1987) discussed the effects of
7 interference between circular cylinders with different array configurations in cross flow, and later
8 the flow interference between four equally spaced cylinders was reported by Sayers (1988, 1990).
9 In addition, Lam and Lo (1992) and Lam and Fang (1995) employed dye injection visualization to
10 obtain the flow pattern of four equispaced cylinders. Subsequently, Lam et al. (2003a, 2003b)
11 conducted further tests to obtain Strouhal number and force coefficients for each cylinder. Recently,
12 Liu et al. (2015a, 2015b) performed experimental and numerical investigations on excitation loads
13 and flow patterns around four circular-section columns and four square-section columns in a square
14 configuration. The main findings of these works indicated that the upstream columns were subjected
15 to higher mean drag forces than the downstream ones, while the downstream columns usually
16 experienced larger fluctuating forces due to unsteady wake vortices from the upstream ones.

17 In the case of semi-submersible platforms, the wake interference dominates VIM response. As
18 characteristic components, both columns and pontoons contribute to complex wake interference and
19 thus have significant effects on the VIM of semi-submersibles. However, few studies have been
20 published concerning the corresponding influences of the pontoons including the fluid physics in
21 terms of the interaction between the multiple vortex shedding processes and VIM behavior. To
22 address this knowledge gap, towing tests were carried out to investigate the VIM performance of

1 DDSs with four pontoons, two pontoons, and no pontoons in order to comparatively analyze the
2 influence of the pontoons. With the objective of capturing the detailed 3-D vortex structures and
3 obtaining full-field instantaneous physical information, flow-induced motion simulations of semi-
4 submersibles were performed using CFD. These two methods, i.e., model tests and CFD, can ideally
5 serve as cross-validation tools for verifying remaining uncertainties.

6

7 **Nomenclature**

8	A_p	submerged projected area
9	A_x	motion amplitude in the in-line direction
10	A_y	motion amplitude in the transverse direction
11	A_{yaw}	yaw motion amplitude
12	B	hull width
13	C	structural damping coefficient
14	C_D	drag force coefficient
15	\bar{C}_D	average drag force coefficient
16	C_L	lift force coefficient
17	C_{Lrms}	root mean square value of the lift force coefficient
18	D	projected width of the column
19	f_0	natural frequency in the transverse direction in calm water
20	f_{0y}	natural frequency of yaw motion in calm water
21	F_x	hydrodynamic force acting on the platform in the in-line direction (or drag force)
22	F_y	hydrodynamic force acting on the platform in the transverse direction (or lift force)

1	H	immersed column height above the pontoon
2	K_x	linear spring constant in the in-line direction
3	K_y	linear spring constant in the transverse direction
4	L	column width
5	L_p	pontoon width
6	m	platform mass
7	P	pontoon height
8	R_c	column radius
9	Re	Reynolds number
10	R_p	pontoon radius
11	S	center-to-center column spacing
12	St	Strouhal number
13	T	draft
14	T_0	natural period in the transverse direction in calm water
15	T_{0y}	natural period of yaw motion in calm water
16	U	current velocity
17	U_r	reduced velocity
18	Δ	platform displacement
19	Δt	time step
20	Δy	distance of the first node away from the hull surface
21	α	current incidence angle
22	ρ	fluid density

1	u_*	wall friction velocity
2	ν	kinematic viscosity coefficient
3	y^+	non-dimensional distance of the first node away from the hull surface

4 2. Experimental arrangement

5 The experiments were conducted in a towing tank rather than an offshore basin, because the
6 towing tank provides smooth flow inlet condition and avoids the uncertain impact of inlet current
7 turbulence. The towing tank has dimensions of 130 m in length, 6 m in width, and 3 m in water
8 depth.

9 2.1 Models of three configurations

10 The models were constructed in accordance with the design of a DDS, with the main dimensions
11 showing in Table 1, based on the dimensions defined in Fig. 1. The DDS has four square columns
12 with four rounded corners each, connected to four square pontoons with four rounded corners each.

13 The scale ratio of the model was 1:64.

14 Table 1

15 Principal dimensions of the deep-draft semi-submersible.

Parameter	unit	value	
		prototype	model
Column width (L)	m	19.5	0.305
Column radius (R_c)	m	3.0	0.047
Pontoon width (L_p)	m	19.5	0.305

Pontoon radius (R_p)	m	2.0	0.031
Immersed column height above the pontoon (H)	m	37.0	0.578
Pontoon height (P)	m	10.0	0.156
Draft ($T=H + P$)	m	47.0	0.734
Center-to-center column spacing (S)	m	72.5	1.133
Hull width ($B=L + S$)	m	92.0	1.438

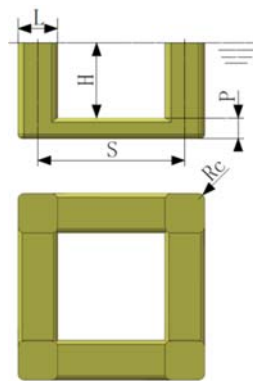


Fig. 1. Characteristic dimensions of a four-column semi-submersible.

In order to acquire sufficient information about the influence of pontoon on VIM response, towing tests were conducted for three configurations (a DDS with four pontoons, a DDS with two pontoons, and a four-column structure with no pontoons), as shown in Fig. 2. All models were bare hulls without any appendages. The main characteristics of three configurations are exactly the same as the DDS in Table 1. In addition, they have the same mass ratio and draft condition as presented in Table 2, which are relevant for VIM of multi-column platforms (Goncalves et al., 2013 and Rijken, 2014).

Table 2

Characteristics of three tested configurations in model scale.

Parameter	Unit	I	II	III
-----------	------	---	----	-----

		DDS	DDS	Four-column structure
		(4 pontoons)	(2 pontoons)	(no pontoons)
Mass (m)	kg	382.3	311.6	241.7
Displacement (Δ)	kg	422.3	344.3	267.0
Mass ratio (m/Δ)	-	0.91	0.91	0.91
Draft (T)	m	0.734	0.734	0.734

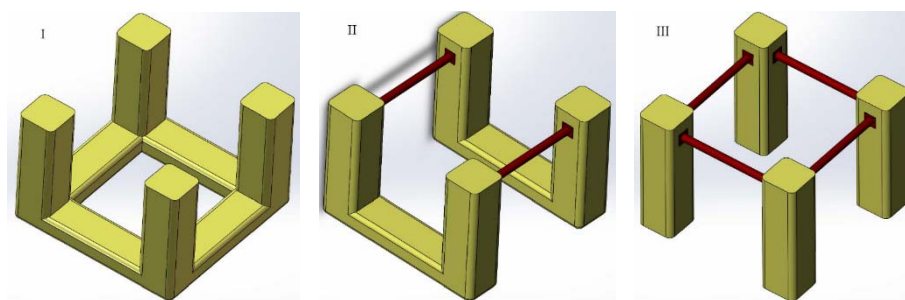


Fig. 2. Schematic view of three tested configurations.

2.2 Model test setup

In the experiment, the hull model was restrained through a set of soft horizontal lines with springs connected to the towing carriage. Fig. 3 shows details of the model test setup. An air bearing system was developed in order to model the vertical pretension arising from the mooring and riser system. The model was equipped with four low-friction air bearings that slid along a smooth horizontal table, which was supported by the towing carriage. The set up ensures that the model was allowed to move freely in the horizontal plane, and vertical motions of the model were restrained. It is inevitable that the VIM observed during the towing test could be affected by the horizontal plane damping due to the friction of the air bearings. Prior to the formal tests, this particular aspect was investigated by the decay test in the air, and the additional damping introduced by the air bearings was found to be less than 1% of the critical damping.

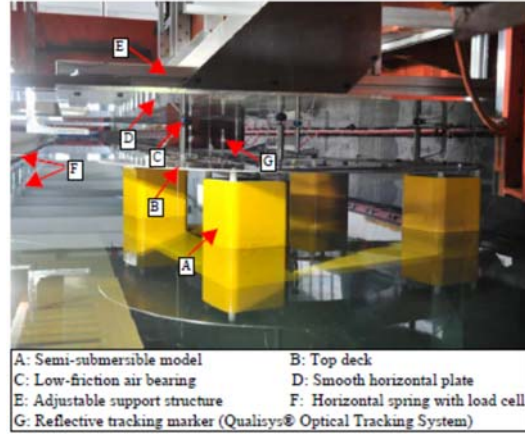


Fig. 3. Model test setup in the towing tank.

The equivalent mooring system, i.e., four soft horizontal lines with springs, was employed to provide the horizontal restoring for the model and to match the natural periods in the horizontal plane. The mooring lines were attached above the water level to avoid disturbing the vortex shedding, as displayed in Fig. 4. Each horizontal line with a load cell was attached to an anchor post on the carriage at one end and to the top deck of the model at the other end. The top deck was built with some studs located at a 15° interval as a ring, which allows the same mooring configuration for all different current incidences.

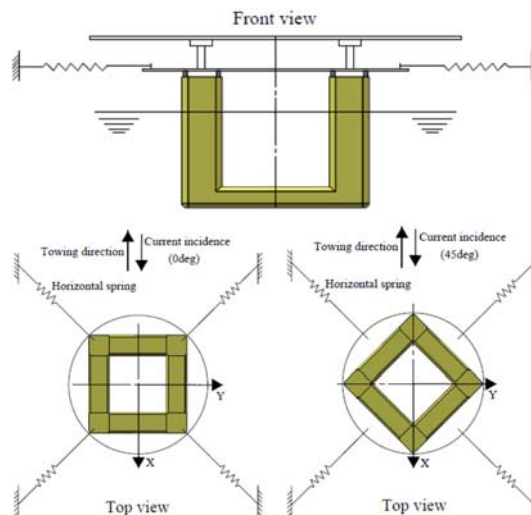


Fig. 4. A schematic layout of the horizontal mooring system.

The X and Y axes represent the global (basin-fixed) coordinate system (Fig. 4). The current flow

came from $-X$, opposite to the towing direction. The angle between each horizontal line and horizontal axes was 45° , and the mooring stiffness of each spring was 30 N/m, which corresponded to the same value of mooring stiffness for in-line and transverse directions.

2.3 Test program and data analysis

Prior to the VIM tests, the static offset test and free-decay tests in calm water were conducted to check the experimental setup and the natural periods of the system, respectively. Table 3 shows the natural periods for each configuration at the tested current incidences.

One of the most important parameters that dominate the VIM response is the reduced velocity (U_r) commonly defined as

$$U_r = (UT_0)/D \quad (1)$$

where U is the incident current velocity, equal to the towing velocity; T_0 is the natural period of the motion in the transverse direction as presented in Table 3; D is the characteristic length of the structure normal to the current and is defined as following based on Fig. 5:

$$D = L(|\sin \alpha| + |\cos \alpha|) \quad (2)$$

where L is the column width and α is the current incidence angle. The projected width (D) tends to govern the width of the wake and is able to better represent the characteristic length of the column section subjected to the current.

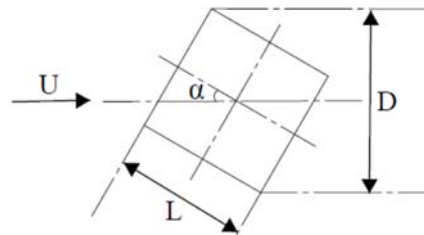


Fig. 5. Definition of projected width (D).

Two current incidences were considered, i.e., 0° and 45° , for all tested configurations. The model-

1 scale current speeds ranged from 0.06 m/s up to 0.31 m/s, corresponding to the Reynolds numbers
2 below 3.0×10^5 in model tests. This is to avoid the uncertainties associated with the transitional
3 flow in the boundary layer of the cylindrical structures. The Froude number was the same in full
4 scale and in model scale, and did not exceed 0.2, similar to typical offshore applications.

5 The results are analyzed by taking the statistics from the time traces and presented in model scale.
6 The characteristic amplitudes of the in-line and transverse motions are non-dimensionalized by the
7 width of the column. The nominal response value is defined as

$$8 \quad (A/L)_{nominal} = \sqrt{2} * std.dev(A)/L \quad (3)$$

9 where A denotes the motion amplitude.

10 In the experiment, the total hydrodynamic forces were derived from the following motion
11 equations for a platform with linear springs and damping in two uncoupled degree-of-freedom as
12 (Sarpkaya, 2004)

$$13 \quad m\ddot{X}(t) + C\dot{X}(t) + K_x X(t) = F_x(t) \quad (4)$$

$$14 \quad m\ddot{Y}(t) + C\dot{Y}(t) + K_y Y(t) = F_y(t) \quad (5)$$

15 where m is the platform mass; C is the structural damping coefficient; K_x and K_y represent the
16 linear spring constant in the in-line, X , and transverse, Y , directions, respectively; $F_x(t)$ and $F_y(t)$
17 are the total hydrodynamic forces acting on the platform in X and Y directions, respectively.

18 The total hydrodynamic force is the sum of the inertial, dissipative and restoring forces of the
19 system in each given direction. According to Goncalves et al. (2012), the structural dissipative force
20 can be disregarded, due to its smaller magnitude than the other forces. Consequently, the total
21 hydrodynamic force is acquired by adding the inertial and restoring forces. The restoring forces of
22 the system, measured by four load cells, are decomposed in the in-line and transverse directions,

1 also taking into account the yaw angle.

2 The hydrodynamic forces in the in-line and transverse directions are represented in the non-
3 dimensional form, namely, the drag coefficient, C_D , and the lift coefficient, C_L , respectively

$$4 \quad C_D(t) = \frac{2F_x(t)}{\rho A_p U^2} \quad (6)$$

$$5 \quad C_L(t) = \frac{2F_y(t)}{\rho A_p U^2} \quad (7)$$

6 where ρ is the fluid density, and A_p is the submerged projected area of the platform as shown in
7 Table 3. The average drag coefficient (\bar{C}_D) and the root mean square value of the lift coefficient
8 (C_{Lrms}) will be discussed, in order to better understand the vortex-shedding behavior and the VIM
9 response.

10 Table 3

11 Natural periods in calm water and submerged projected areas for the tested configurations at
12 different current incidences. Values are in model scale.

Configuration	Current incidence, α	Natural period in the transverse direction, T_0 (s)	Natural period of yaw motion, T_{0y} (s)	Submerged projected area, A_p (m^2)
I. DDS (4 pontoons)	0°	19.4	17.1	0.577
	45°	20.1	18.3	1.065
II. DDS (2 pontoons)	0°	19.1	19.0	0.448
	45°	19.0	18.7	1.065
III. Four-column structure	0°	16.3	17.2	0.448
(no pontoon)	45°	16.7	16.9	0.950

3. Numerical simulation

Computational Fluid Dynamics (CFD) approach is often applied to solve the coupled rigid body motions for a floating platform together with the fluid transport equations owing to improvements in both hardware and software. Previous uses of CFD in spar VIM predictions have shown promising results. Building on this, 3-D numerical simulations on the flow-induced motion of semi-submersibles were performed for comparison against the experimental results and for more detailed investigation on the fluid physics associated with VIM in terms of wake characteristics and interaction, and vortex dynamics.

3.1 Numerical model and simulation scheme

The numerical simulations were carried out at the same model scale, regardless of geometric imperfections in the actual model from fabrication tolerances in the physical model tests. The dimensions and characteristics of the three CFD models, i.e., a DDS with four pontoons, a DDS with two pontoons, and a four-column structure with no pontoons, can be found in Tables 1 and 2. The arrangement of the mooring system and the mooring stiffness in the CFD simulations were the same as those in the model test setup.

All numerical simulations presented in this paper were performed with the finite volume CFD code STAR-CCM+ provided by CD-adapco. There are currently three approaches for simulating the motion of the structure. Dynamic Fluid-Body Interaction (DFBI) Rotation and Translation Motion is a particular motion feature often used for (but not restricted to) marine applications; the rotations of which are expected to be small. To simulate the VIM of semi-submersibles, DFBI was applied to all simulations. In this approach, the semi-submersible is meshed within a large

surrounding volume mesh and the entire mesh moves along with the semi-submersible without mesh distortion.

The high Reynolds number leads to turbulent flow around the semi-submersible model. The VIM of semi-submersibles is governed by the oscillating hydrodynamic forces arising from large-scale turbulent eddies. Thus, it is critical to resolve the large-scale eddies in the wake of semi-submersibles. Lefevre et al. (2013) discussed the applicability of unsteady Reynolds' Averaged Navier-Stokes (RANS) and Detached Eddy Simulation (DES) to the spar VIM, and revealed that the Spalart-Allmaras (SA)-DES turbulence model can provide very good prediction in amplitude values as those reported in towing tests, which were much better than those of predicted by the Shear Stress Transport (SST) K-Omega model. In essence, the SA-DES model treats the flow as a RANS simulation in the boundary layer by applying the SA model and as a Large Eddy Simulation (LES) calculation elsewhere. Therefore, it tends to be much more economical than a true LES simulation, which requires a much finer mesh in the boundary layer. From this point forward, the SA-DES turbulence model was utilized to capture turbulence effects in this study.

3.2 Computational domain and boundary conditions

In order to avoid side wall effects, the computational domain is chosen as 25.88 m long (i.e., 6 times the hull width upstream and 12 times the hull width downstream), 17.25 m wide (i.e., 12 times the hull width), and 4.40 m deep (i.e., 6 times the model draft) based on the convergence study, as presented in Fig. 6. In previous numerical studies on the VIM of semi-submersibles, the size of the computational domain varied slightly. For example, the computational domain was $14B \times 12B \times 4.5T$ (length \times width \times depth, respectively) in the study by Kim et al. (2011) and $27B \times 18B \times 6T$ in the study by Tan et al. (2013). In contrast, Lee et al. (2014) performed VIM simulations using a

1 computational domain with a length of $5B$, width of $4B$ and depth of $2.2T$.

2 The boundary conditions applied to the calculations were a velocity inlet at the flow inlet, a
3 pressure outlet at the flow outlet, symmetry planes at the domain bottom and the two lateral walls,
4 and a non-slip wall on the hull surface (see Fig. 6). The free surface was fixed at the mean water
5 level as a symmetry plane, owing to the low Froude number obtained in both the model tests and
6 CFD simulations. Only the motions in the horizontal plane are considered, i.e., the heave, row, and
7 pitch, are neglected due to their very small magnitude for a semi-submersible in current environment
8 and are not expected to affect the VIM behavior.

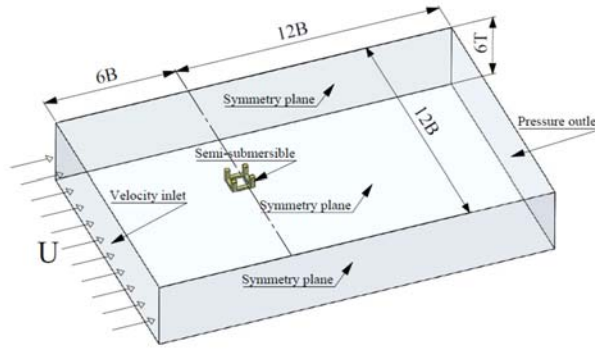
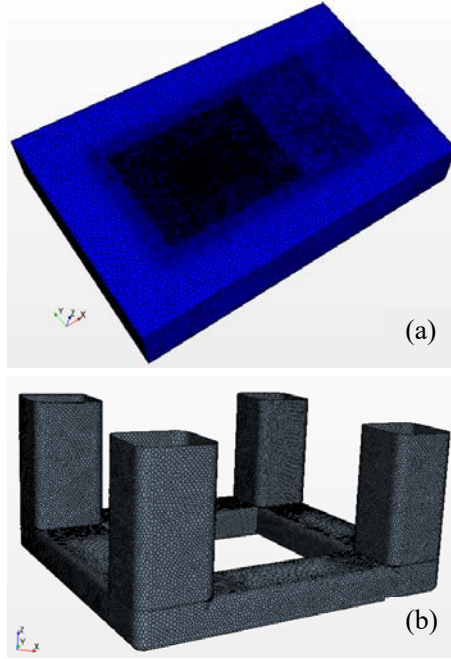


Fig. 6. Computational domain and boundary conditions.

11 3.3 Convergence tests and validation

12 A polyhedral mesh has been utilized throughout the water region, as presented in Fig. 7. The mesh
13 on the hull surface is sized to capture the boundary layer. The values of y^+ , which represents the
14 non-dimensional distance of the first node away from the hull surface, were less than 1 over the
15 entire wall boundary; namely, $y^+ = u_* \Delta y / \nu$, where u_* denotes the wall friction velocity, ν
16 denotes the kinematic viscosity coefficient, and Δy is the distance of the first node from the hull
17 surface. The wake behind the semi-submersible must be adequately resolved to capture the larger
18 eddies, which are vital to driving the oscillating hydrodynamic forces. Thus, the other key mesh-

1 sizing requirement is the wake resolution.



2
3 Fig. 7. An example of the mesh: (a) whole computational domain; (b) hull surface mesh.

4 Both grid and time step convergence tests were performed for the DDS with four pontoons at a
5 45° -incidence, and the reduced velocity, U_r , is 6.58. Table 4 shows the results of convergence tests
6 with four meshes and four time steps, where the relative change represents the variation of two
7 consecutive cases. The statistical quantities of the hydrodynamic results are calculated from 15
8 response cycles after the response repeating itself. Small variations are observed in the average drag
9 force coefficients (\bar{C}_D) even though the number of mesh elements is different. Comparing the results
10 of Cases M2 and M3, both the response amplitude in the transverse direction and the RMS of the
11 lift coefficient (C_{Lrms}) show a great increase (i.e., the variations are 8.93% and 16.42%, respectively)
12 as the number of mesh elements increases. However, the differences between the results of Cases
13 M3 and M4 are always less than 5%.

14 The influence of the time step on the numerical results was evaluated by comparing the results
15 from Cases T1 to T4 (where T3 is the same as case M3). The variations both in the motion amplitude

and \bar{C}_D between different time steps are below 2%. The fluctuating lift force coefficient also shows negligible differences. Moreover, similar results were obtained when performing calculations with smaller time steps. It is apparent that the smaller time step increases the computational time of the simulation. In consideration of the accuracy and efficiency, all VIM simulations were performed on the ‘M3’ mesh with a non-dimensional time step of 0.005.

Table 4

Results of the cases with different grid and time resolutions.

Case No.	No. of cells (million)	$\Delta t/T_0$	A_y/L	Relative change	Relative \bar{C}_D	Relative change	C_{Lrms}	Relative change
M1	0.88	0.005	0.646	-	1.284	-	0.224	-
M2	1.45	0.005	0.671	3.76%	1.321	2.84%	0.232	3.50%
M3	3.74	0.005	0.737	8.93%	1.343	1.63%	0.278	16.42%
M4	5.60	0.005	0.760	1.73%	1.345	0.16%	0.290	4.02%
T1	3.74	0.010	0.757	-	1.317	-	0.308	-
T2	3.74	0.007	0.743	1.90%	1.337	1.49%	0.298	3.27%
T3	3.74	0.005	0.737	0.84%	1.343	0.45%	0.278	7.23%
T4	3.74	0.002	0.739	0.25%	1.342	0.10%	0.268	3.56%
Exp.	-	-	0.742	-	1.413	-	0.269	-

Additionally, the results of the model tests are also given in Table 4. Slight deviations in the response amplitude and hydrodynamic forces are observed between Case M3 and the experiment. Therefore, the three-dimensional numerical simulations presented in this study are reliable.

4. Results and discussion

1 Towing tests and numerical simulations on the three configurations have been carried out to
2 examine the influence of pontoons on the VIM of DDSs.

3 4.1 Response in the transverse direction

4 Fig. 8 presents the results of normalized motion amplitudes in the transverse direction for
5 different configurations obtained from the model tests and simulations. It can be clearly seen that
6 the numerical results are in good agreement with the experimental measurements, a further
7 validation of the numerical model after rigorous convergence tests.

8 For each configuration, the DDS under the current at the 45° -incidence shows much larger VIM
9 amplitudes in the transverse direction than responses of DDS under the current at a 0° -incidence. At
10 the 0° -incidence, similar trend and values in the motion amplitudes are observed for the DDS with
11 four pontoons and the DDS with two pontoons. A small peak with A_y/L near 0.2 occurs in the
12 range of $5 < U_r < 8$ for these two semi-submersibles, and the amplitudes slightly increase at
13 higher U_r ($U_r > 12$). Additionally, the response amplitudes of the four-column structure with no
14 pontoons show a similar trend but with higher values.

15 The motion amplitudes in the transverse direction for the three configurations under the current
16 at a 45° -incidence are rather similar in trend, i.e., they attain their respective peak values in the same
17 range ($5 < U_r < 8$) as observed at a 0° -incidence and then decrease sharply to a stable value. This
18 confirms the existence of a resonant behavior for the VIM of semi-submersibles and four-column
19 structures for a range of reduced velocities, i.e., lock-in scenario. The largest VIM amplitudes in the
20 transverse direction with values $A_y/L \cong 0.9$ are observed for the four-column structure at a 45° -
21 incidence. On the other hand, the DDS with four pontoons and the DDS with two pontoons show
22 the same maximum A_y/L values, which are approximately 0.7.

According to these results, the four-column structure with no pontoons shows more significant motion in the transverse direction at both 0°- and 45°-incidences. Consulting previous studies on four-column arrays arranged in a square configuration (Lam et al., 2003b and Liu et al., 2015a), when the spacing ratio (S/L) is above 4.00, the wake from each column is well established. In the present investigation, the spacing ratio of the three configurations is approximately 3.72. However, the presence and position of the pontoons promote a great modification in the wake of the columns, and there is significant interference between the column and the pontoon in the cases of DDSs with either four pontoons or two pontoons. Consequently, a loss in the shedding synchronization occurs leading to reduced motion in the transverse direction (Fig. 8).

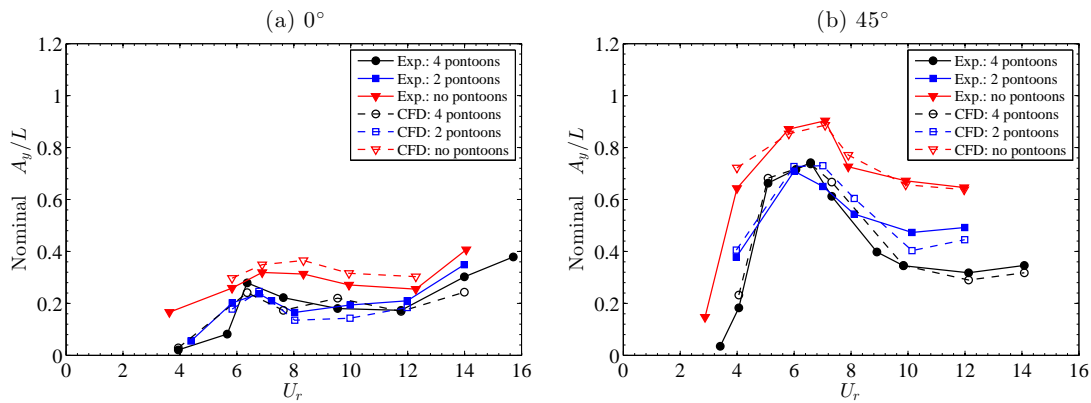


Fig. 8. Non-dimensional amplitudes of the motion in the transverse direction for the three different configurations at 0°- and 45°-incidences.

The RMS values for the lift force coefficient obtained from the numerical simulations at a 45°-incidence (see Fig. 9) show good agreement with the results calculated from the model tests. The largest fluctuating lift force coefficient, with a value of approximately 1.1, occurs at $U_r \cong 4$ for the four-column structure, which corresponds to the most significant motion in the transverse direction. In comparison with the four-pontoon DDS, the DDS with two pontoons shows a larger lift force for higher U_r ($U_r \geq 8$), and consequently induces more pronounced VIM response in the

transverse direction.

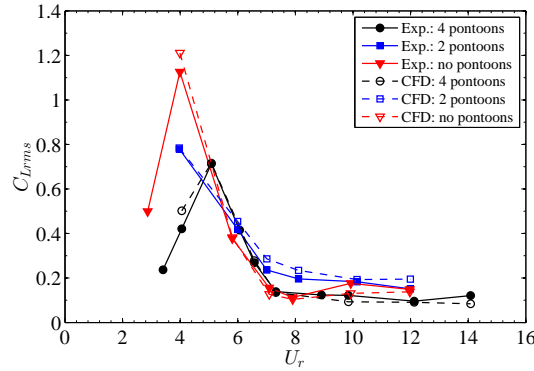
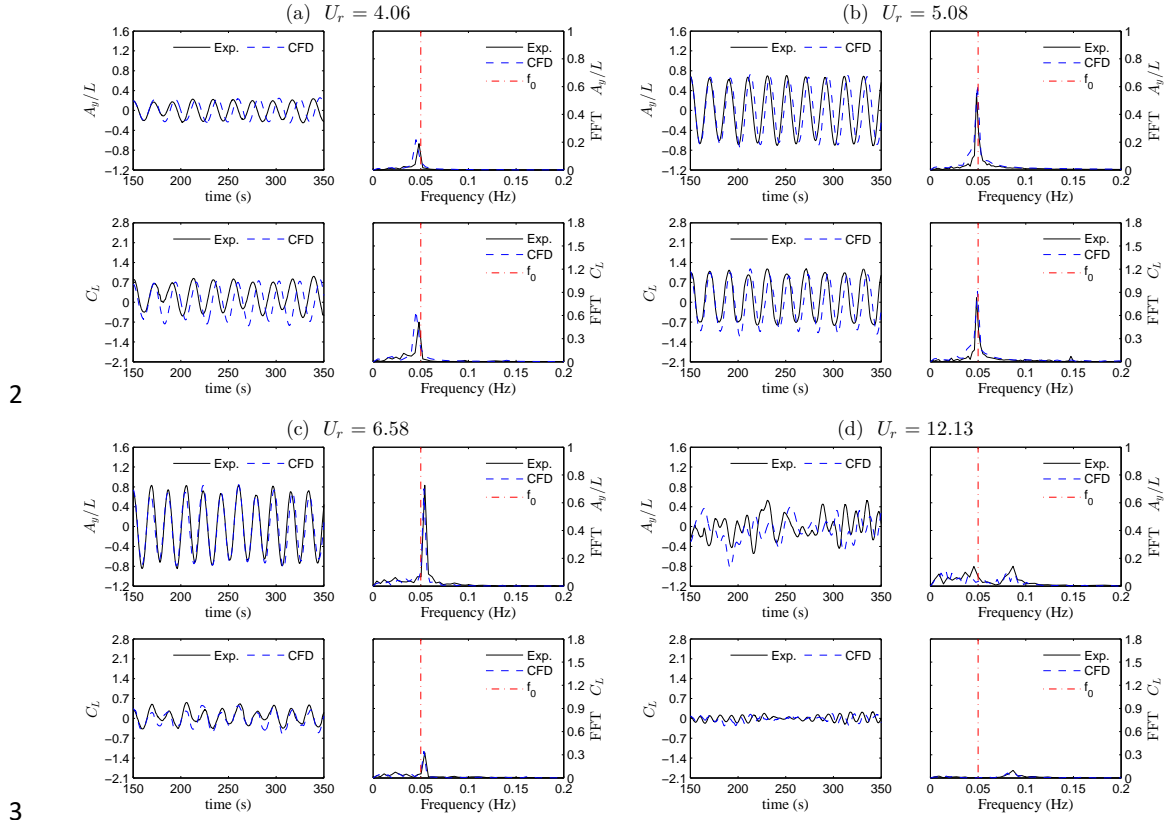


Fig. 9. Lift force coefficient for the three different configurations at a 45°-incidence.

Fig. 10 presents the time history and results of spectral analysis via FFT for the motion in the transverse direction and the lift force coefficient of the DDS with four pontoons at a 45°-incidence. The time scale is at model scale, and the initial transient data has been removed to process the statistics.

It can be seen that the motions synchronize with the lift force coefficients for different reduced velocities. This corroborates that the fluctuating transverse lift force governs the motion in the transverse direction. For $5 < U_r < 8$, i.e., Fig 10(b) and (c), the motions show the largest amplitudes with well-defined oscillation frequencies. Additionally, the dominant frequencies are around the natural frequency of transverse motion in calm water (f_0), which confirms the resonance behavior (lock-in) for the transverse motion in this range of reduced velocities. Fig. 10(a) shows that the transverse response presents a smaller motion amplitude with a dominant oscillation frequency for $U_r = 4.06$, corresponding to a region before synchronization in the transverse direction, i.e., pre-lock-in scenario. In contrast, Fig. 10(d) shows the time histories and spectral analysis for the post-lock-in scenario ($U_r = 12.13$). At this reduced velocity, the motion in the transverse direction does not present a characteristic periodicity, i.e., no obvious single oscillation

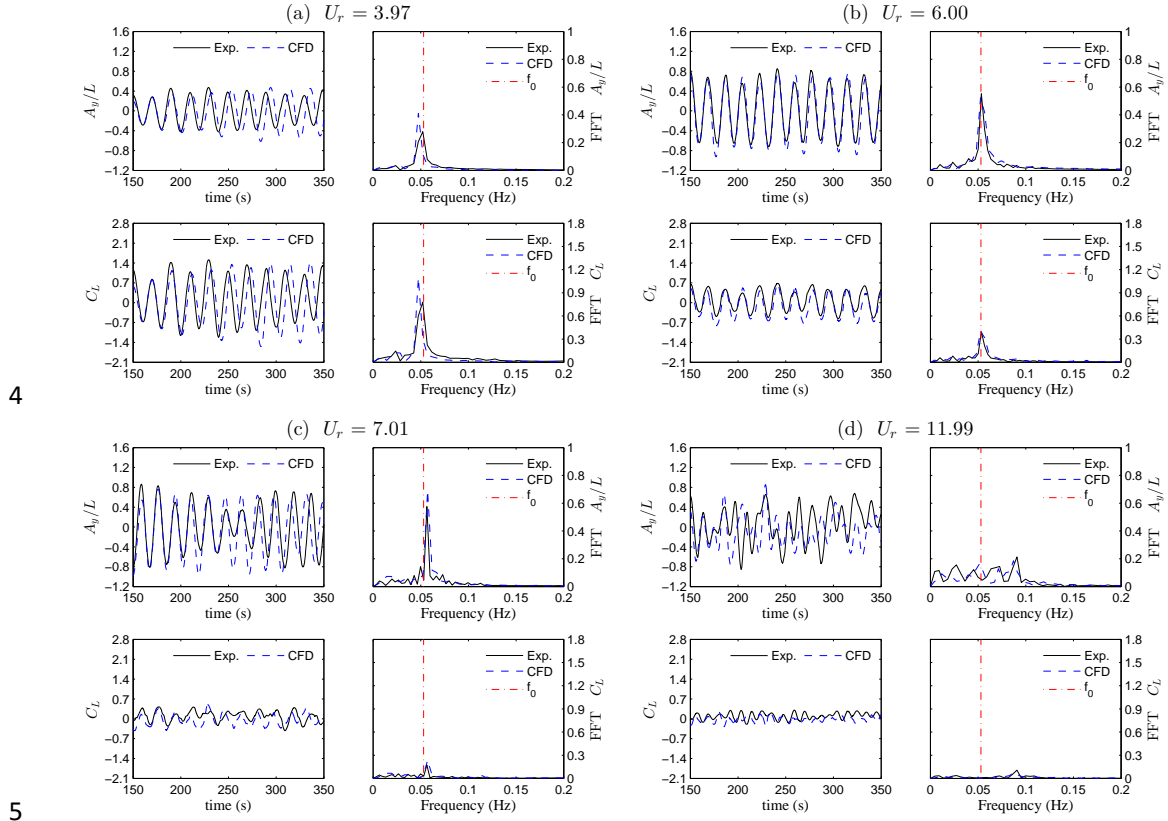
1 frequency can be defined.



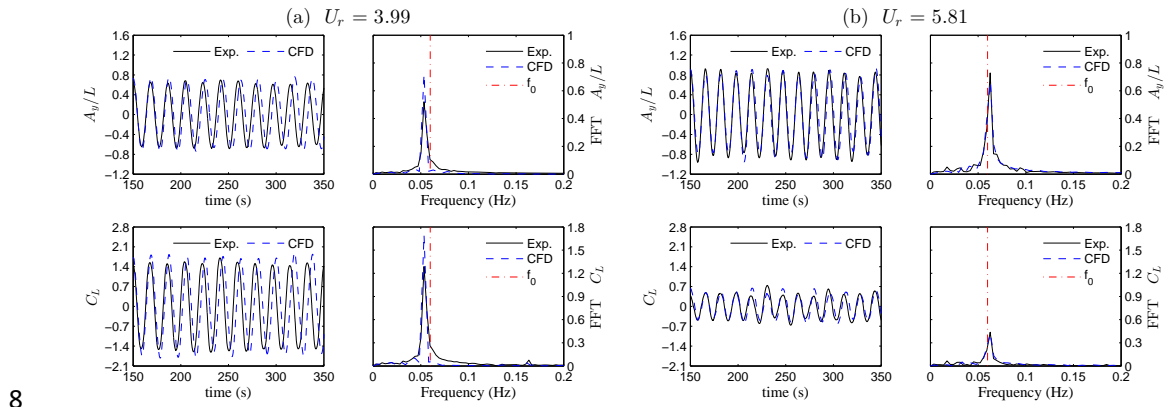
2
3
4 Fig. 10. Time history and spectral analysis for the motion in the transverse direction and the lift
5 force coefficient of the DDS with four pontoons at a 45°-incidence.

6 In the same way, the time history and results of spectral analysis for the DDS with two pontoons
7 and the four-column structure with no pontoons are shown in Figs. 11 and 12, respectively.
8 Synchronization regions of the transverse motion are also observed for these two configurations, as
9 identified in the case of the four-pontoon DDS. However, large amplitude motions concentrated
10 around the respective transverse natural frequencies can be seen for the DDS with two pontoons at
11 $U_r = 3.97$ and for the four-column structure at $U_r = 3.99$, as presented in Figs. 11(a) and 12(a),
12 respectively. The resonance phenomenon for these two configurations seems to occur at a lower
13 reduced velocity in comparison with the four-pontoon DDS, indicating that the presence of pontoons
14 defers VIM behavior until reaching a high reduced velocity. Moreover, the four-column structure

1 shows the largest amplitudes of the transverse motion and the highest lift force coefficient in the
 2 range of the reduced velocities, i.e., the presence of pontoons verifiably reduces the transverse
 3 responses.



4
 5
 6 Fig. 11. Time history and spectral analysis for the motion in the transverse direction and the lift
 7 force coefficient of the DDS with two pontoons at a 45°-incidence.



8

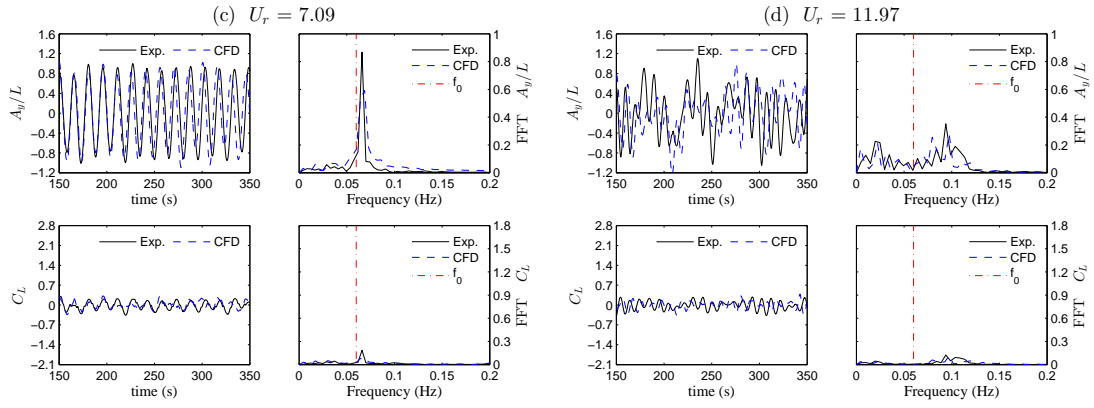


Fig. 12. Time history and spectral analysis for the motion in the transverse direction and the lift force coefficient of the four-column structure with no pontoons at a 45°-incidence.

4.2 Response in the in-line direction

Fig. 13 presents the normalized motion amplitudes in the in-line direction for different configurations obtained from the model tests and numerical simulations. The semi-submersibles and the four-column structure, exposed to a steady current, are subjected to in-line drag forces. Therefore, the in-line motion appears at a new equilibrium location, away from the hydrostatic position, that depends on drag forces. Obviously, the motions in the in-line direction are less significant with much smaller magnitude compared to the response in the transverse direction. According to these results, the motion amplitudes in the in-line direction tend to increase slightly with the increase in the reduced velocity at a 0°-incidence. The in-line motion amplitude also presents an upward trend at a 45°-incidence, but a larger amplitude of $A_x/L \approx 0.2$ in $6 < U_r < 8$ is found for the DDS with two pontoons, which may be attributed to the presence of asymmetric pontoons.

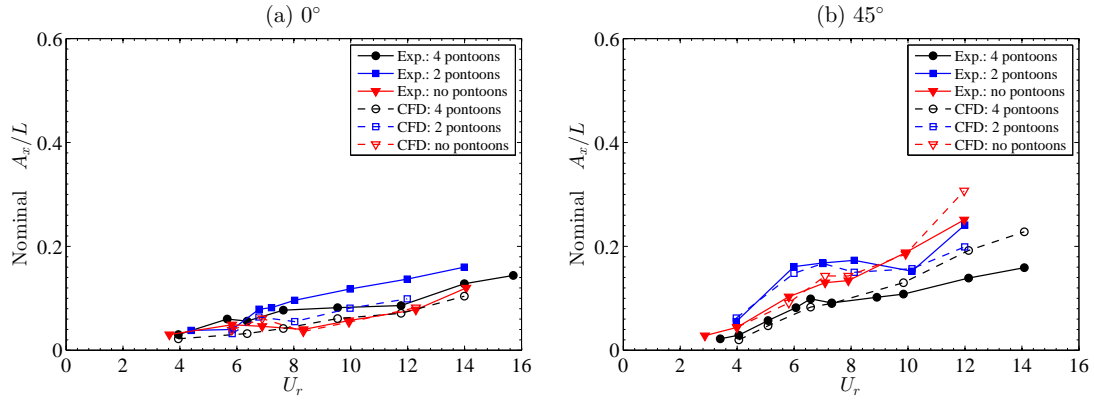
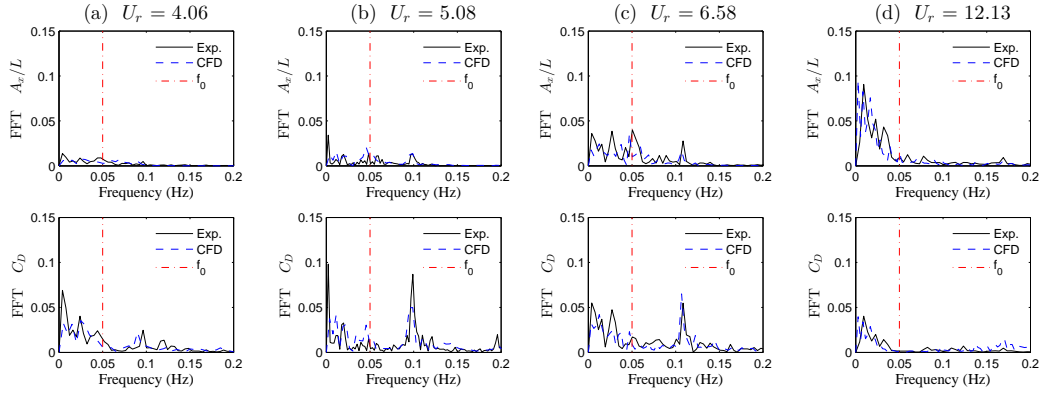


Fig. 13. Non-dimensional amplitudes of the motion in the in-line direction for the three different configurations at 0°- and 45°-incidences.

In order to better understand the response in the in-line direction, examples of spectral analysis for the motion in the in-line direction and the drag force coefficient of the three different configurations at a 45°-incidence are presented in Figs. 14-16. In comparison to the response in the transverse direction, the motion in the in-line direction involves diverse components and shows more random characteristics. Moreover, the in-line characteristic amplitudes are rather small owing to drag forces oscillating in a negligibly small range. However, the dynamic drag forces mainly occur around frequencies twice those of the respective lift force oscillating frequencies, especially for the DDS with four pontoons and the four-column structure at $U_r < 10$, which are in accordance with investigations into flow around cylindrical structures (see Sumer and Fredsøe, 1997). It is important to highlight that for the DDS with two pontoons at $U_r < 10$, the in-line motions and the drag forces are less pronounced periodic oscillations, and the dominant frequencies are approximately equal to the respective frequencies of the transverse response at different reduced velocities. Therefore, in the synchronization range of the transverse response, the motion in the in-line direction oscillates with the same frequency as the transverse motion, and a complex coupling between the in-line and transverse response may appear. These are very likely to promote the in-

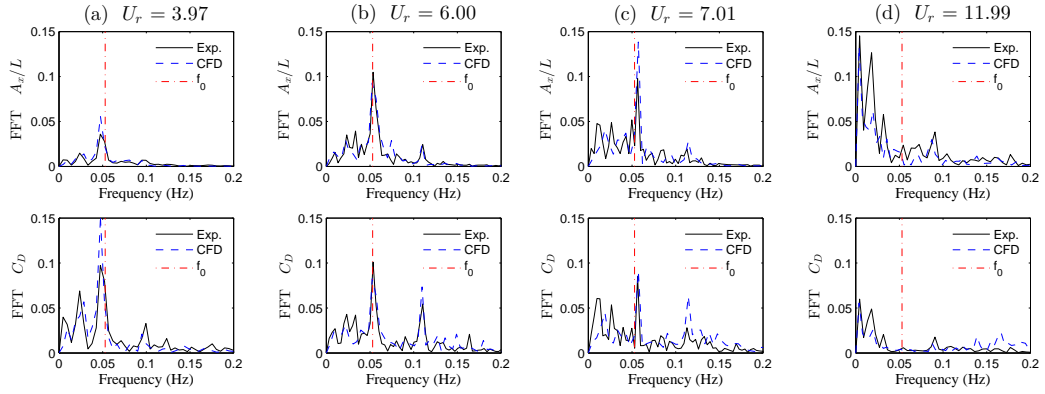
1 line motion of the two-pontoon semi-submersible.



2

3 Fig. 14. Spectral analysis for the motion in the in-line direction and the drag force coefficient of

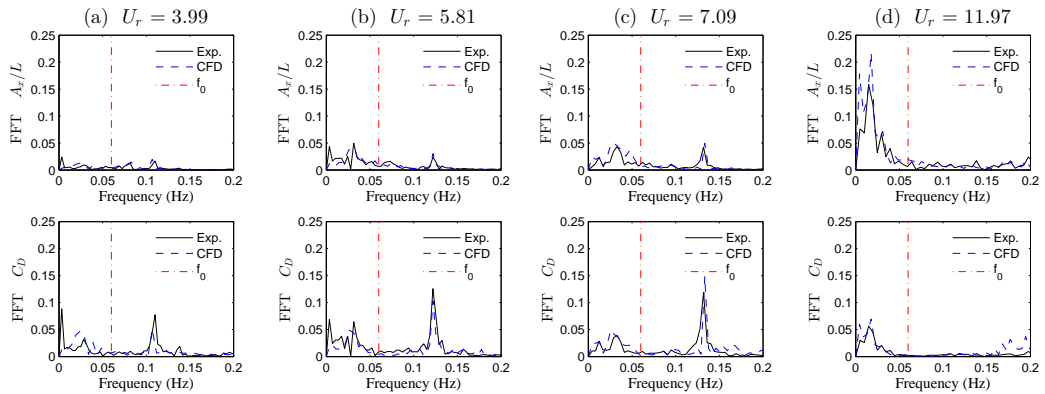
4 the DDS with four pontoons at a 45°-incidence.



5

6 Fig. 15. Spectral analysis for the motion in the in-line direction and the drag force coefficient of

7 the DDS with two pontoons at a 45°-incidence.



8

9 Fig. 16. Spectral analysis for the motion in the in-line direction and the drag force coefficient of

10 the four-column structure with no pontoons at a 45°-incidence.

4.3 Yaw response

Fig. 17 shows nominal yaw amplitudes for the three different configurations. A similar trend and approximate amplitudes in the yaw response can be found for all configurations at a 0° -incidence, but the yaw amplitudes of the four-column structure are slightly larger. The yaw amplitudes reach peak values between 4.5° and 5° in the range of $5 < U_r < 8$ for all configurations, and then decrease sharply. This observation confirms the existence of resonant phenomenon on yaw response. According to these results, the presence of pontoons appears to have only a small effect on the yaw motion at a 0° -incidence.

However, the pontoons exert a more noticeable influence for the 45° -incidence. The four-column structure with no pontoons shows the largest yaw amplitudes. Additionally, the yaw motions of the four-column structure for 0° - and 45° -incidences are similar in both trends and values, reaching their maxima in $5 < U_r < 8$. A similar trend of yaw motion with smaller amplitudes is observed for the DDS with two pontoons at a 45° -incidence. The yaw amplitudes of the DDS with four pontoons at the 45° -incidence show a gradual increase until $U_r > 8$, and then remain at a stable level. The fluctuating moment though not presented here, owing to different values of drag and lift forces for each column and pontoon, is likely responsible for the yaw motion. Further research is required to better understand the influence of pontoons on the yaw response.

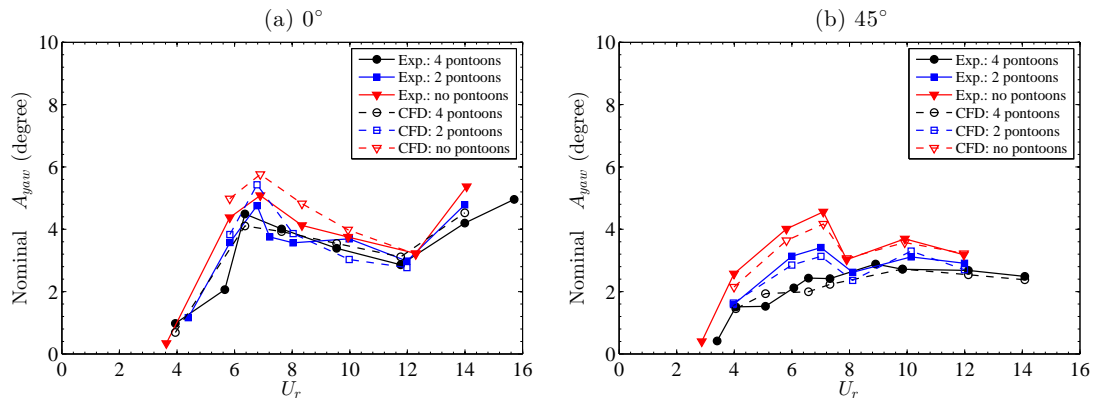


Fig. 17. Yaw characteristic amplitudes for the three different configurations at 0°- and 45°- incidences.

Examples of spectral analysis for the yaw motion of the three different configurations at a 45°- incidence are presented in Figs. 18-20. The yaw responses of semi-submersibles in the range $4 \leq U_r < 8$ are periodic but less regular in comparison with the transverse motions. The dominant frequencies are around the respective natural frequencies of the yaw motion (f_{0y}), which corroborates the resonance behavior for the yaw motion of semi-submersibles in this range of reduced velocities. In contrast, the four-column structure shows more periodic yaw response with larger amplitudes in the same range, and the yaw motions are concentrated around the natural frequency of the yaw response in still water. This fact also confirms the resonance phenomenon for the yaw motion of the four-column structure. It is evident that the level of irregularity increase as U_r increases. For higher U_r , the yaw responses of all configurations are irregular, i.e., no dominant frequency can be defined.

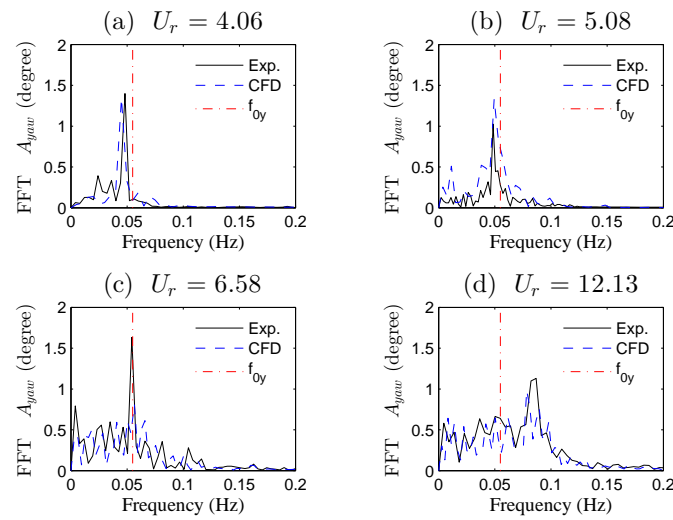


Fig. 18. Spectral analysis for the yaw motion of the DDS with four pontoons at a 45°-incidence.

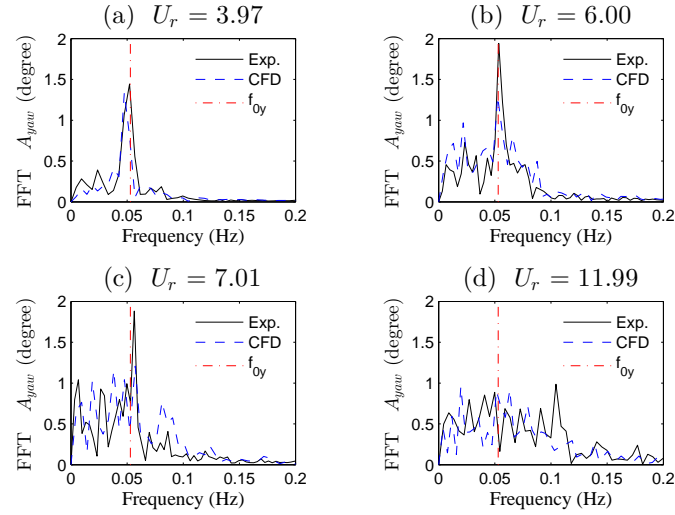


Fig. 19. Spectral analysis for the yaw motion of the DDS with two pontoons at a 45°-incidence.

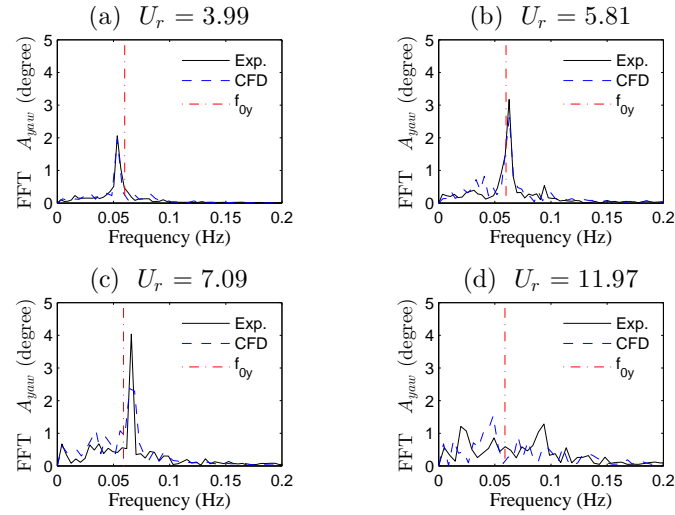


Fig. 20. Spectral analysis for the yaw motion of the four-column structure with no pontoons at a 45°-incidence.

4.4 Motion trajectory in the XY plane

The motion trajectories in the XY plane are plotted in Figs. 21-23 in order to better understand VIM behaviors of the semi-submersibles and the four-column structure, respectively. Since the good agreement has been shown in the experimental and numerical results, only motion trajectories obtained from model tests are presented in this section.

There are no eight-shaped trajectories observed as those typically presented in the VIM of spar

1 and monocolumn platforms. The VIM responses of the semi-submersibles and the four-column
2 structure occur primarily along one of the hull diagonals for the 45°-incidence (Figs. 21-23). The
3 overall drag on the structures increased as the reduced velocity became larger, which resulted in the
4 increased offset. In the synchronization region, the lock-in phenomenon with pronounced transverse
5 amplitudes is observed for all configurations. The four-column structure shows the largest
6 amplitudes of motion in the transverse direction, and the transverse responses for two semi-
7 submersibles are of similar magnitude. However, the in-line responses of the DDS with two
8 pontoons are more significant in this range, and the trajectory is more like a cocoon (Fig. 22).

9 Moreover, the response of the DDS with four pontoons is limited at $U_r \leq 4$, but the responses of
10 the other two configurations are noticeable at the same range of U_r , especially for the four-column
11 structure. This implies that the presence of pontoons delays the onset of VIM to a higher reduced
12 velocity.

13 The motions of semi-submersibles and the four-column structure appear more random for post
14 lock-in conditions (i.e., higher U_r). It is worth noting that the magnitude of the in-line response is
15 as pronounced as the transverse component at the highest U_r tested for all three configurations.
16 For the design of the semi-submersible, it would be prudent to take the in-line and transverse effects
17 into consideration. The differences between the responses of all configurations are more or less
18 obvious owing to the existence of pontoons.

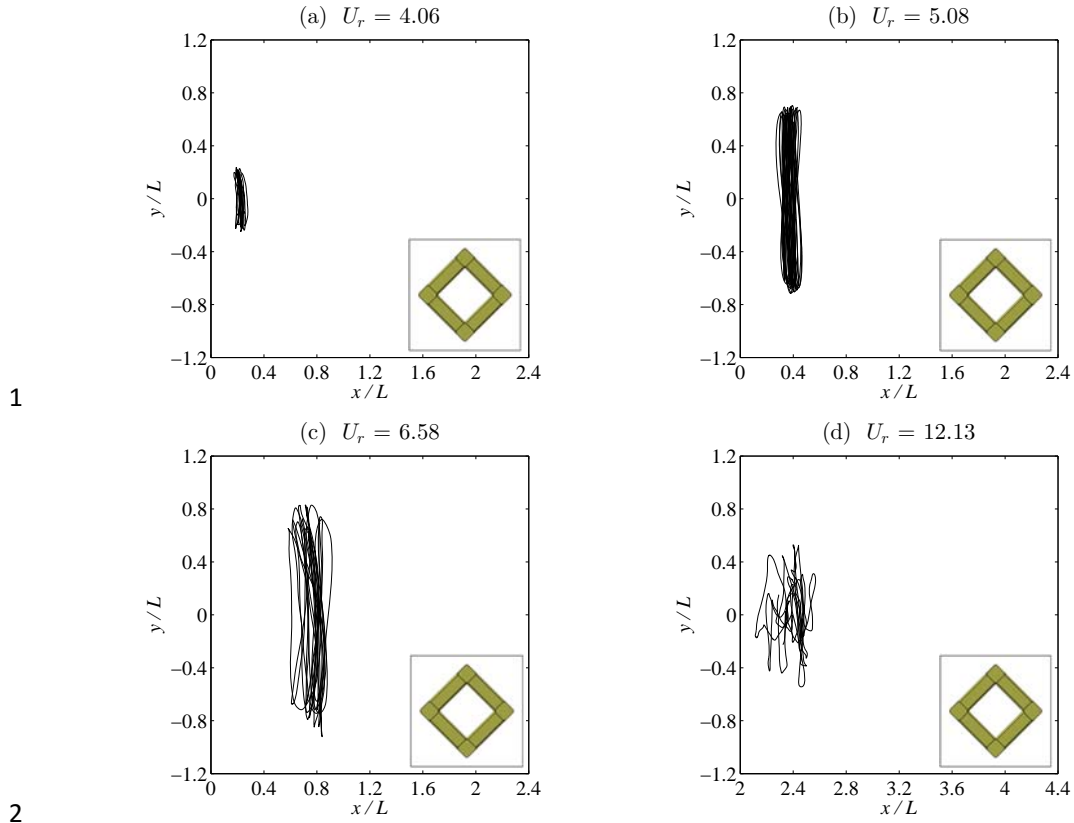


Fig. 21. Motion trajectories in the XY plane for the DDS with four pontoons at a 45° -incidence.

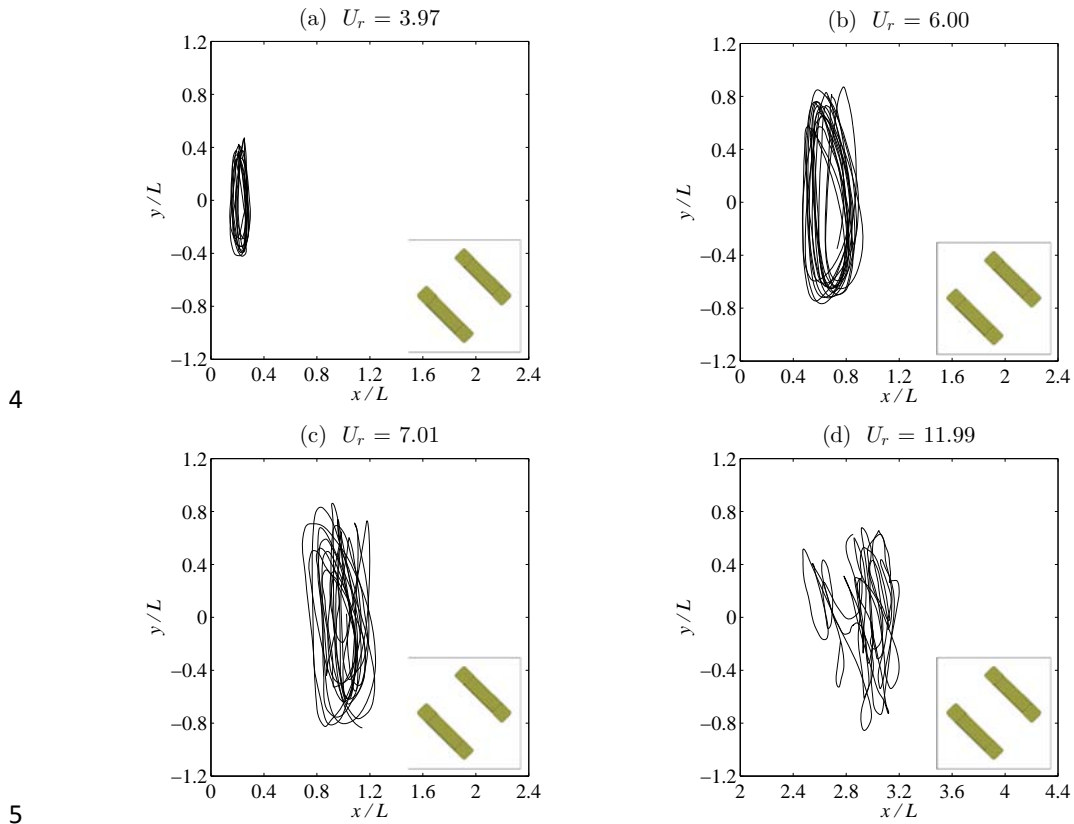


Fig. 22. Motion trajectories in the XY plane for the DDS with two pontoons at a 45° -incidence.

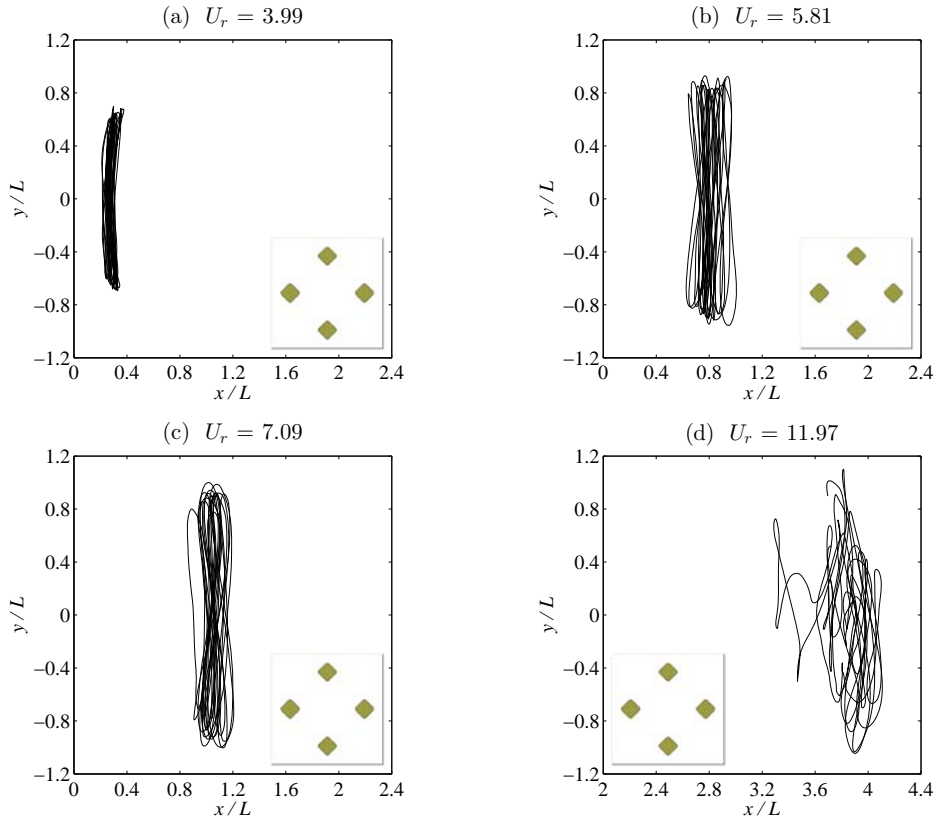


Fig. 23. Motion trajectories in the XY plane for the four-column structure with no pontoons at a 45° -incidence.

4.5 Instantaneous flow field

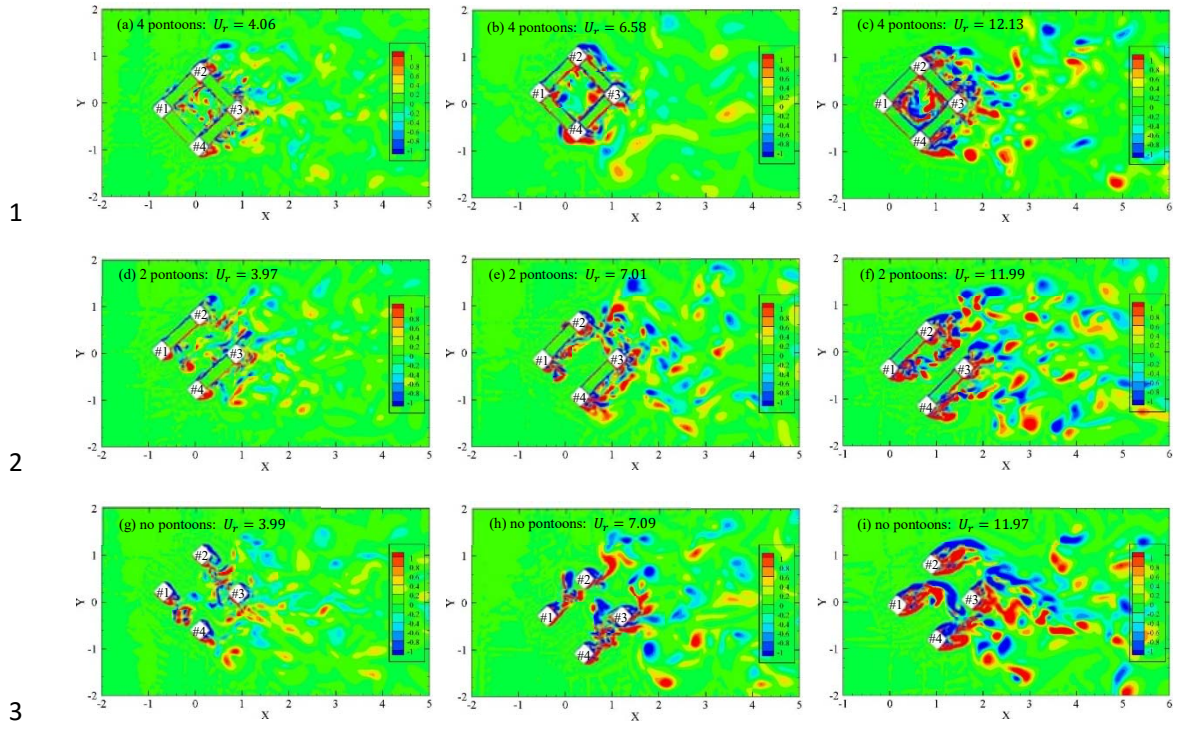
After verification against the experimental data from model tests, the 3-D numerical simulation are conducted to further reveal the fluid physics with quantitative information, which is extremely difficult to obtain experimentally. Flow patterns play a vital role in the behavior of the pressure distribution around structures, especially for the instantaneous fluctuating pressure. This has a significant effect on the characteristics of flow-induced forces, which govern the VIM of semi-submersibles and the four-column structure. As shown in Figs. 24 and 25, the flow pattern characteristics at a 45° -incidence are clearly illustrated by vorticity contours.

In the pontoon-top-surface plane (i.e., $Z = P$), the influence of the pontoon on the vorticity field is obvious. The vortex shedding around the upstream column (#1) is partly trapped and subsequently

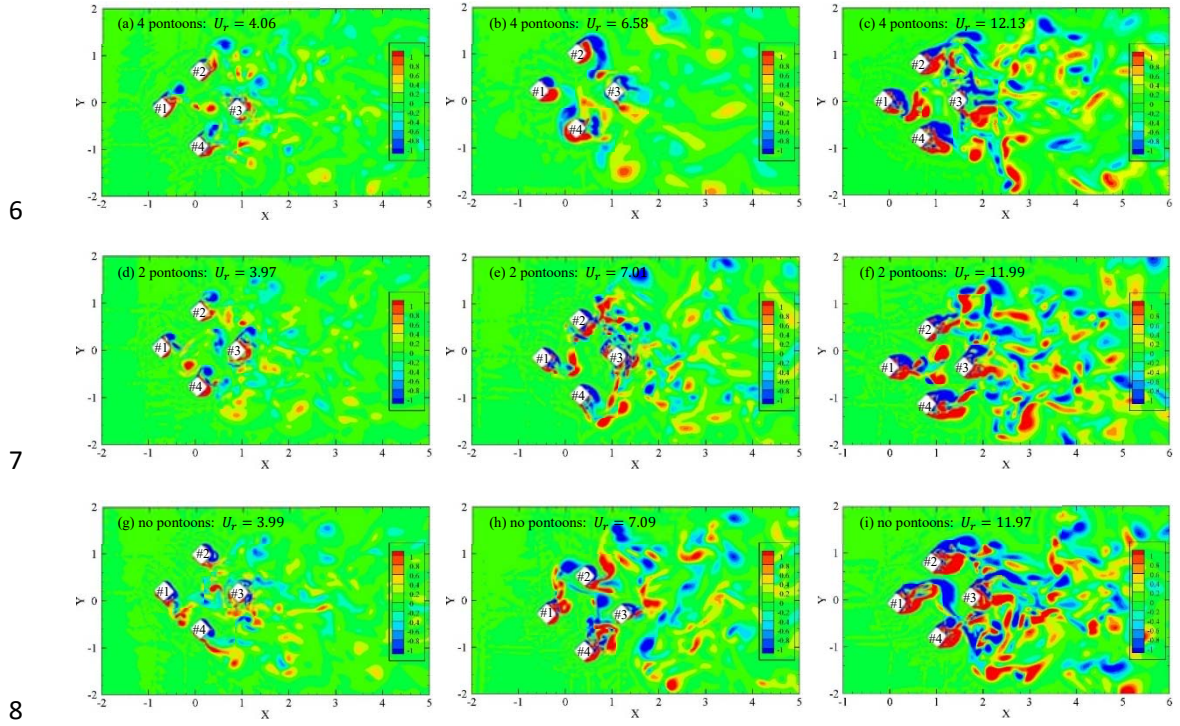
1 suppressed considerably due to the pontoons immersed in its wake (see Fig. 24 a-c), for the four-
2 pontoon DDS cases. Non-alternating vortices shed at the outward edges of the lateral columns (#2
3 and #4), which lead to the decrease in oscillatory lift forces, implying reduced VIM response.
4 Additionally, the vortices from the pontoons lead to a disordered flow field with strong vortices not
5 shedding in the region between the pontoons for the four-pontoon DDS, especially at high reduced
6 velocities, corresponding to more random and less significant motions.

7 For the DDS with two pontoons, the vortex shedding occurs on one side of both the upstream
8 column (#1) and the lateral column (#4), while vortices shed from two sides of the lateral column
9 (#2) alternately. However, both the lateral column (#2) and the downstream column (#3) are clearly
10 affected by vortex shedding from the upstream column and pontoon. Thus, the transverse response
11 of the two-pontoon semi-submersible are partly mitigated in comparison with that of the four-
12 column structure with no pontoons. It is important to highlight that for the DDS with two pontoons,
13 the lateral columns (#2 and #4) are located asymmetrically in the current owing to the asymmetric
14 presence of pontoons at a 45° -incidence, implying the different wake of these two columns. This is
15 likely to contribute to the more pronounced motions in the in-line direction.

16 Pontoon effects are not noticeable in the XY plane at $Z = T/2$ as shown in Fig. 25. In all three
17 cases, vortex shedding occurs around the far corners away from the column centerline, and the
18 vortices shed from the columns in phase together. Moreover, the vortices shedding from the columns,
19 which vary with the flow characteristics around stationary cylinders, are not along the in-line
20 direction owing to the motions of the semi-submersibles and the four-column structure. Therefore,
21 interactions between the flow and the structure are observed.



4 Fig. 24. Instantaneous vorticity contour plots in the XY plane at $Z = P$ (pontoon height) for all
5 configurations at a 45° -incidence.



9 Fig. 25. Instantaneous vorticity contour plots in the XY plane at $Z = T/2$ (half draft) for all
10 configurations at a 45° -incidence.

5. Conclusions

Aiming to examine the influence of pontoons on the VIM of semi-submersible platforms, the VIM behaviors of two DDSs and a four-column structure were investigated both experimentally and numerically. Model tests were carried out with equivalent horizontal springs and an air-bearing system in a towing tank. The 3-D numerical simulations were performed using DES. Based on the analysis of comprehensive results on VIM and flow characteristics, the following conclusions are drawn from the present study.

The transverse motions for each configuration at a 45° -incidence are more pronounced than those at a 0° -incidence. However, the 0° -incidence current tends to induce more marked yaw responses.

Resonance behavior in the transverse direction is observed at reduced velocities ranging from 5 to 8 for the DDS with four pontoons, while the synchronization regions for the two-pontoon DDS and the four-column structure range from 4 up to 8. The presence of pontoons delays the onset of VIM to a higher reduced velocity.

The largest amplitudes of motion in the transverse direction are observed for the four-column structure owing to the well-established wake of each column without the influence of the pontoons. For higher reduced velocities, the strong vortices from the pontoons lead to disordered flow in the region between the pontoons of the four-pontoon DDS, whereas the two pontoons are directed into the undisturbed flow in cases of the two-pontoon DDS. Thus, the DDS with two pontoons can generate larger lift forces at higher reduced velocities, corresponding to more significant motion in the transverse direction compared with the four-pontoon DDS.

For the semi-submersibles and the four-column structure, the in-line motion is less clear and more random than the transverse motion. The motion trajectories in the XY plane are primarily along the

hull diagonal at a 45° -incidence. However, for the DDS with two pontoons, the dominant frequency of the drag force matches that of lift force, implying the coupling between the in-line and transverse responses. This likely promotes the in-line motion of the two-pontoon semi-submersible.

Acknowledgements

The authors would like to thank the support of the National Natural Science Foundation of China (Grant No.51279104) and a research project on high-technology ships supported by the Ministry of Industry and Information Technology.

References

- Finn, L.D., Maher, J.V., Gupta, H., 2003. The cell spar and vortex induced vibrations. In: Proceedings of the Offshore Technology Conference (OTC 2003), Houston, USA, OTC2003-15244.
- Finnigan, T., Irani, M., Van Dijk, R., 2005. Truss Spar VIM in Waves and Currents. In: Proceedings of the 24th International Conference on Offshore Mechanics and Arctic Engineering, Halkidiki, Greece, OMAE2005-67054.
- Gonçalves, R., Franzini, G., Fajarra, A., Meneghini, J., 2010a. Two degrees-of-freedom vortex-induced vibration of a circular cylinder with low aspect ratio, Sixth Conference on Bluff Body Wakes and Vortex-Induced Vibrations, Capri Island, Italy.
- Gonçalves, R.T., Fajarra, A.L.C., Rosetti, G.F., Nishimoto, K., 2010b. Mitigation of vortex-induced motion (VIM) on a monocolumn platform: forces and movements. J. Offshore Mech. Arctic Eng. 132 (4), 041102.
- Goncalves, R.T., Rosetti, G.F., Fajarra, A.L.C., Oliveira, A.C., 2012. Experimental study on vortex-

1 induced motions of a semi-submersible platform with four square columns, Part I: Effects of
2 current incidence angle and hull appendages. *Ocean Eng.* 54, 150-169.

3 Goncalves, R.T., Rosetti, G.F., Fajarra, A.L.C., Oliveira, A.C., 2013. Experimental study on vortex-
4 induced motions of a semi-submersible platform with four square columns, Part II: Effects of
5 surface waves, external damping and draft condition. *Ocean Eng.* 62, 10-24.

6 Hong, Y., Choi, Y., Lee, J., Kim, Y., 2008. Vortex-induced motion of a deep-draft semi-submersible
7 in current and waves. In: *Proceedings of the 18th International Offshore and Polar Engineering*
8 *Conference*, Vancouver, BC, Canada.

9 Huang, K., Chen, X., Kwan, C.T., 2003. The impact of vortex-induced motions on mooring system
10 design for spar-based installations. In: *Proceedings of the Offshore Technology Conference*
11 *(OTC 2003)*, Houston, USA, OTC2003-15245.

12 Irani, M., Finn, L., 2004. Model testing for vortex induced motions of spar platforms. In:
13 *Proceedings of the 23th International Conference on Offshore Mechanics and Arctic*
14 *Engineering*, Vancouver, British Columbia, Canada, OMAE2004-51315.

15 Irani, M., Finn, L., 2005. Improved strake design for vortex induced motions of spar platforms. In:
16 *Proceedings of the 24th International Conference on Offshore Mechanics and Arctic*
17 *Engineering*, Halkidiki, Greece, OMAE2005-67384.

18 Kim, J.-W., Magee, A., Guan, K.Y.H., 2011. CFD simulation of flow-induced motions of a multi-
19 column floating platform. In: *Proceedings of the 30th International Conference on Ocean,*
20 *Offshore and Arctic Engineering*, Rotterdam, The Netherlands.

21 Lam, K., Fang, X., 1995. The effect of interference of four equispaced cylinders in cross flow on
22 pressure and force coefficients. *J. Fluids Struct.* 9 (2), 195-214.

1 Lam, K., Li, J.Y., Chan, K.T., So, R.M.C., 2003a. Flow pattern and velocity field distribution of
2 cross-flow around four cylinders in a square configuration at a low Reynolds number. *J. Fluids*
3 *Struct.* 17 (5), 665-679.

4 Lam, K., Li, J.Y., So, R.M.C., 2003b. Force coefficients and Strouhal numbers of four cylinders in
5 cross flow. *J. Fluids Struct.* 18 (3), 305-324.

6 Lam, K., Lo, S.C., 1992. A visualization study of cross-flow around four cylinders in a square
7 configuration. *J. Fluids Struct.* 6 (1), 109-131.

8 Lee, S.-K., Chien, H.-P., Gu, H., 2014. CFD Study of Deep Draft SemiSubmersible VIM. *Offshore*
9 *Technology Conference-Asia. Offshore Technology Conference.*

10 Lefevre, C., Constantinides, Y., Kim, J.W., Henneke, M., Gordon, R., Jang, H., Wu, G., 2013.
11 Guidelines for CFD Simulations of Spar VIM. In: *Proceedings of the 32nd International*
12 *Conference on Ocean, Offshore and Arctic Engineering, Nantes, France, OMAE2013-10333.*

13 Liu, M., Xiao, L., Kou, Y., Wu, F., 2015a. Experimental and numerical studies on the excitation
14 loads and vortex structures of four circular section cylinders in a square configuration. *Ships*
15 *Offshore Struct.*, 1-13.

16 Liu, M., Xiao, L., Yang, L., 2015b. Experimental investigation of flow characteristics around four
17 square-cylinder arrays at subcritical Reynolds numbers. *Int. J. Nav. Archit. Ocean Eng.* 7 (5),
18 906-919.

19 Ma, W., Wu, G., Thompson, H., Prislin, I., Maraju, S., 2013. Vortex induced motions of a column
20 stabilized floater, *Proceedings of the DOT International Conference*, pp. 22-24.

21 Oakley, O.H., Constantinides, Y., 2007. CFD truss spar hull benchmarking study. In: *Proceedings*
22 *of the 26th International Conference on Offshore Mechanics and Arctic Engineering, San*

1 Francisco, California, USA, OMAE2007-29150.

2 Rijken, O., 2014. Examining the effects of scale, mass ratios and column shapes on the vortex
3 induced motion response of a semisubmersible through CFD analyses. In: Proceedings of the
4 33rd International Conference on Ocean, Offshore and Arctic Engineering, San Francisco,
5 California, USA, OMAE2014-23471.

6 Rijken, O., Leverette, S., 2008. Experimental study into vortex induced motion response of semi
7 submersibles with square columns. In: Proceedings of the 27th International Conference on
8 Offshore Mechanics and Arctic Engineering, Estoril, Portugal, OMAE2008-57396.

9 Rijken, O., Leverette, S., 2009. Field measurements of vortex induced motions of a deep draft
10 semisubmersible. In: Proceedings of the 28th International Conference on Ocean, Offshore and
11 Arctic Engineering, Honolulu, HI, USA, OMAE2009-79803.

12 Rijken, O., Schuurmans, S., Leverette, S., 2011. Experimental investigations into the influences of
13 SCRs and appurtenances on DeepDraft Semisubmersible Vortex Induced Motion response. In:
14 Proceedings of the 30th International Conference on Ocean, Offshore and Arctic Engineering,
15 Rotterdam, The Netherlands, OMAE2011-49365.

16 Sagrilo, L.V.S., de Siqueira, M.Q., de Lacerda, T.A.G., Ellwanger, G.B., de Lima, E.C.P., Siqueira,
17 E.F.N., 2009. VIM and wave-frequency fatigue damage analysis for SCRs connected to
18 monocolumn platforms. In: Proceedings of the 28th International Conference on Ocean,
19 Offshore and Arctic Engineering, Honolulu, HI, USA, OMAE2009-79431.

20 Sarpkaya, T., 2004. A critical review of the intrinsic nature of vortex-induced vibrations. *J. Fluids*
21 *Struct.* 19 (4), 389-447.

22 Sayers, A.T., 1988. Flow interference between four equispaced cylinders when subjected to a cross

1 flow. J. Wind Eng. Ind. Aerodyn. 31 (1), 9-28.

2 Sayers, A.T., 1990. Vortex shedding from groups of three and four equispaced cylinders situated in
3 a cross flow. J. Wind Eng. Ind. Aerodyn. 34 (2), 213-221.

4 Sumer, B.M., Fredsøe, J., 1997. Hydrodynamics around cylindrical structures. World Scientific.

5 Tan, J.H.C., Magee, A., Kim, J.W., Teng, Y.J., Zukni, N.A., 2013. CFD Simulation for Vortex
6 Induced Motions of a Multi-Column Floating Platform. In: Proceedings of the 32nd
7 International Conference on Ocean, Offshore and Arctic Engineering, Nantes, France,
8 OMAE2013-11117.

9 van Dijk, R.R.T., Voogt, A., Fourchy, P., Mirza, S., 2003. The effect of mooring system and sheared
10 currents on vortex induced motions of truss spars. In: Proceedings of the 22nd International
11 Conference on Offshore Mechanics and Arctic Engineering, Cancun, Mexico, OMAE2003-
12 37151.

13 Waals, O.J., Phadke, A.C., Bultema, S., 2007. Flow Induced Motions on Multi Column Floaters. In:
14 Proceedings of the 26th International Conference on Offshore Mechanics and Arctic
15 Engineering, San Francisco, California, USA, OMAE2007-29539.

16 Wang, Y., Yang, J.-m., Lü, H.-n., 2009. Computational fluid dynamics and experimental study of
17 lock-in phenomenon in vortex-induced motions of a cell-truss spar. Journal of Shanghai
18 Jiaotong University (Science) 14, 757-762.

19 Wang, Y., Yang, J., Peng, T., Lu, H., 2010. Strake design and VIM-suppression study of a cell-truss
20 spar. In: Proceedings of the 29th International Conference on Ocean, Offshore and Arctic
21 Engineering, Shanghai, China, OMAE2010-20225.

22 Yung, T.W., Sandström, R.E., Slocum, S.T., Ding, J.Z., Lokken, R.T., 2004. Advancement of spar

- 1 VIV prediction. In: Proceedings of the Offshore Technology Conference (OTC 2004), Houston,
- 2 USA, OTC2004-16343.
- 3 Zdravkovich, M.M., 1987. The effects of interference between circular cylinders in cross flow. J.
- 4 Fluids Struct. 1 (2), 239-261.